FIRST RESULTS OF THE GROUNDTEST OF A FIBRE REINFORCED CONTINUOUS FLEXIBLE GAP AND STEPLESS SMART DROOP NOSE FOR HIGH LIFT APPLICATIONS

M. Kintscher, H. P. Monner, J. Riemenschneider, M. Wiedemann,
Institute of Composite Structures and Adaptive Systems,
Lilienthalplatz 7, 38108 Braunschweig, Germany

Abstract

In order to reduce the airframe noise during landing and the drag in cruise flight, a smart droop nose is a good alternative compared to conventional high lift devices like slats at the leading edge of an aircraft. Furthermore a gap and step less high lift device at the leading edge can be seen as pioneering technology for natural laminar flow application at the wing and further drag reduction in the future. In the framework of the fourth German national research program in aeronautics a smart leading edge was developed by the partners Airbus, EADS-IW, CASSIDIAN and the DLR. The presented paper shows the first results of a 1:1 ground test of a 3D fiber reinforced continuous flexible smart droop nose section for high lift applications. The paper illustrates and explains the concept of the smart droop nose and the test setup of the ground test. Subsequently first results of the ground test i.e. measurements of the deformation behavior of the leading edge at maximum deflection angle will be presented. The deformation at maximum deflection angle will then be compared to the results of finite element simulations with subsequent discussion of deviations. Finally the overall performance of the leading edge segment and deviations from the calculated results will be discussed and assessed.

1. INTRODUCTION

To meet the ambitious goals defined in the VISION 2020, technologies to consequently reduce drag and airframe noise will be necessary. The recommendations of the ACARE group for the reduction of emissions per passenger kilometers are CO2 < 50%, NOx < 80% and noise < 50% until 2020 (ACARE, 2008). To achieve the targeted values new aircraft concepts and with it new concepts for high lift devices have to be developed. The developed systems have to comply with the next generation aircraft requirements like high surface quality and lightweight design. In conventional high lift configurations, devices on leading and trailing edges open slots to achieve the additional lift. However, especially the slots at the leading edge have been identified as the dominant source of airframe noise in approach [2], [3]. Although there is a chance to reduce the slat noise by re-arranging the overlap and gap in combination with an increased salt chord, nevertheless the steps and gaps remaining in retracted position do not comply with requirements for high quality surfaces for future aircraft airfoil design. Regarding the objective of drag reduction, most experts agree that laminarization is the only technology which has the potential for step changes in drag reduction within a suitable timeframe. Current projects dealing with natural laminar flow (NLF) like TELFONA, show promising results for drag reduction up to -12% for the wing [4]. Thus, it is probable that the next generation of wings will employ high aspect-ratios with slim profiles and high quality surfaces like already investigated e.g. within the project NACRE under the acronym HARLS (High Aspect-Ratio Low Sweep), [5]. Because of the gap which forms between the slat and the main wing when retracted, the flow at conventional high lift devices is disturbed and causes transition to turbulent flow immediately after the slat gap. Additionally, the construction space in the next generation high aspect ratio wings is limited due to the employment of slim profiles. Thus, smart seamless and gapless high lift devices especially at the wings leading edge are a mandatory enabler for future wings of significantly increased aerodynamic efficiency and reduced acoustic intensity (Fig. 1).

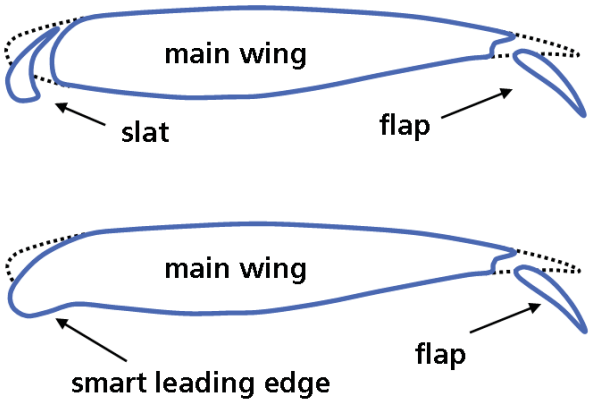

Fig. 1: Conventional high lift configuration and configuration with smart droop nose.

The European and national projects SADE (Smart High Lift Devices for Next Generation Wings) and SmartLED (Smart Leading Edge Device) as well as part of the European funded "Joint Technology Initiative" Clean Sky (Smart Fixed Wing Aircraft, SFWA) are aiming for a major step forward in the development and evaluation of the

potential of morphing airframe technologies. In the national project SmartLED a smart leading edge was developed and tested in 1:1 ground test. The first result from the ground test are presented and discussed in this paper.

2. CONCEPT

There are numerous patents and concepts starting from the early 20s dealing with mechanics and kinematics for the deformation of parts of the airfoil or the complete airfoil. The majority of these patents considers the inner mechanism for the deformation of the airfoil as key issue and assumes a flexible skin not specified otherwise. An example for the leading edge is shown in Fig. 2.

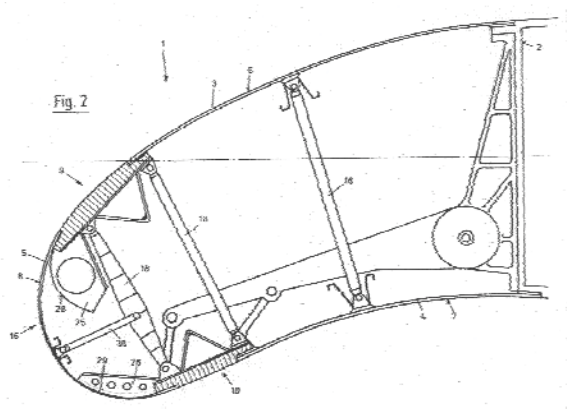

Fig. 2: Patent DE2907912-A1, Dornier Company, 1979.

But today's transportation aircrafts operate at high Mach numbers with high take off weight and much increased surface loading on the wing. Therefore, the kind of the skin and its stiffness and stability properties play a decisive role in the design of morphing structures today. Up to now the maturity of concepts for morphing skins is low and no satisfying solution for the incorporation of stiffness, stability and at the same time flexibility is found [7]. Because of the continuity of the skin while morphing, a downward deflection for example of the device leads to stretching of the upper skin while the lower skin is compressed. A suitable skin has to provide elasticity for the deformation and stiffness at the same time. This is often described as the problem of the adverse requirements for an elastic skin. Therefore a lot of patents and concepts especially for the trailing edge suggest a slotted skin design. The slotted design relaxes the problem of high strains in upper and lower skin. Just as well concepts for the leading edge skin solve this problem in the same way by accepting a discontinuous skin. Although this approach relaxes the problem of high strains in the skin of the device, a disadvantage is the significant stiffness reduction of the structure leading to complex and heavy kinematics. However, due to the evolving gap or step in the slotted lower skin this approach is not compatible with the high surface quality required for laminar flow applications.

The advantage especially for concepts at the leading edge with a continuous end-to-end skin is the continuity of the airfoils shape: In contrast to the kinematics of a trailing edge, the leading edge can be designed in a way that the first buckling mode nearly represents the desired drooped shape of the leading edge. So the buckling or bulging of the structure induced by an actuator force can be used to re-arrange the structure of the leading edge tip. In this case the buckling is a natural reaction of the structure gaining for a status of minimum deformation energy which leads often to an increasing tip radius when the device is deployed. With this knowledge a design philosophy for the design of the smart leading edge aiming at minimum restraint of the smart structure in the desired shape change is adopted from Campanile, [8], and further developed. A patent with the best agreements concerning this kind of design philosophy is the Patent DE 2907912 A1 of the Dornier Company [6] in Fig. 2. In the national project SmartLED this patent was therefore chosen as starting point for the investigation of a smart high lift device at the leading edge.

2.1. Baseline Wing

The baseline wing for the development of the smart leading edge device is the FNG wing (Next Generation Wing) which was released by Airbus within the LuFo ProHMS project for research activities. The wings planform and design is similar to a medium range single-aisle aircraft like the A320. In Fig. 3 the selected section for the design of the smart droop nose is positioned just after the kink at the inner part of the outer wing and is a typical section for the application of a conventional slat. The realistic distribution of leading edge thickness, sweep and tapering is considered as a major challenge for the design of the device. Therefore the selected design wing section is a 3D section. The front spar position as a major geometrical constraint for the design varies in the selected section from 20.4% to 23.7% local clean chord. As a major design issue for gapless high lift devices, the tapering and twist of the wing varies in the selected section like in realistic leading edge sections and is not constant.

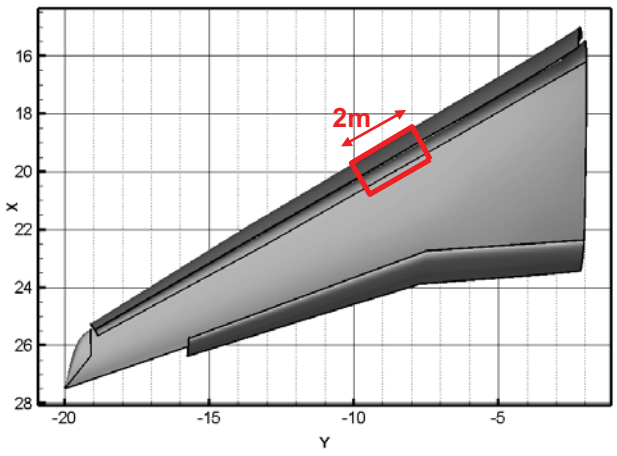

Fig. 3: Baseline FNG wing with selected section for SmartLED application.

2.2. Concept Design

The chosen concept of minimum restraint of the smart structure for the smart droop nose leads to a design process in which the design of the actuator and kinematics is coupled with the design of the flexible structure and can not be handled separately. Further information about the design process, boundary conditions and optimization strategies can be found in [9] and [10].

Finally the resulting smart leading edge design concept consists of a monolithic, flexible glass fiber skin with tailored stiffness in chord direction and omega shaped stringers in span direction. The actuator forces for deformation of the skin are transferred into the skin by an especially designed kinematical chain which is compatible to the desired structural deformation. The omega shaped stringers in this configuration act as stiffeners in span direction but also as interface between the skin and the kinematics. In Fig. 4 the result of a finite element simulation of the chosen concepts is presented. Critical strains can be found in the outer fiber layers of the skin at the leading edge tip. Because pure bending deformation of the monolithic skin is assumed, the strains in the skin correlate directly with the skins thickness. Therefore the skin thickness is the most important design variable in the detailed design of the concept.

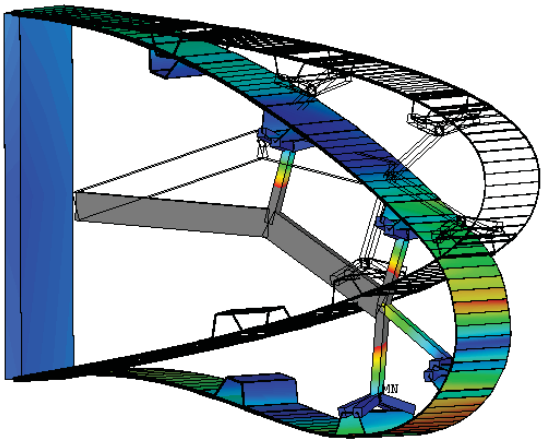

Fig. 4: FE simulation of SmartLED concept, critical strains at the LE tip.

In order to control the critical strains in the skin the skin thickness distribution is chosen in a way that the minimum skin thickness of one millimeter is used at the critical locations at the leading edge tip. Furthermore the fiber orientation and layup is optimized with respect to strength requirements.

3. TEST SETUP

The main objective of the 1:1 ground test of the smart leading edge structure was the demonstration of the feasibility of a smart gap and step less high lift device for the leading edge of a transportation aircraft with conventional flight certified materials and a conventional actuation concept.

3.1. Test Rig

Beside the deformation of the leading edge structure in the desired position without aerodynamic loads one further main issue of the ground test is the assessment of the deformation behavior of the smart structure under relevant wing bending.

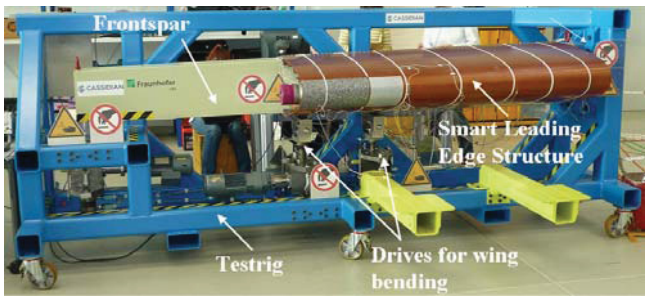

Fig. 5: Test setup with test-rig, test (front) spar and smart leading edge structure.

Therefore a test rig (Fig. 5) was designed by CASSIDIAN (formerly EADS-MAS) which provides the option for simulation of relevant wing bending deformations. The test-rig consists of a rectangular test spar which presents the wing front spar on which the smart leading edge skin is attached via assembly battens. The test spar is build up in an aerospace typical way and consists of riveted side walls, booms, ribs and frames made of aluminum. The test spar is mounted to the test-rig on the side with the larger cross section. For the simulation of wing bending in the ground test the bending line can be set by two drives and one hand wheel for the setting of deformations in z-direction of the test spar according to predefined wing bending lines.

In the smart leading edge, there are four kinematic stations in span direction which were developed by EADS-IW in the SmartLED project.

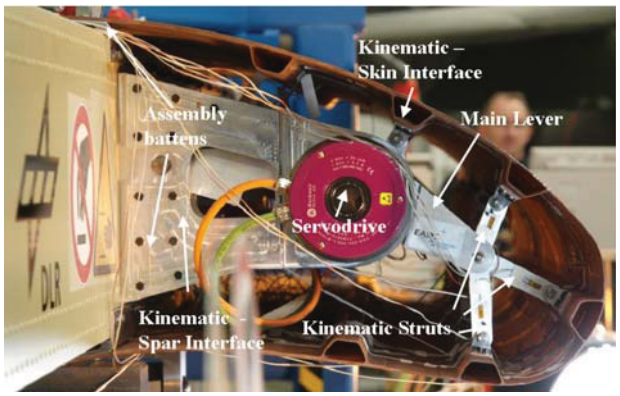

Fig. 6: Kinematics with actuators in the smart leading edge structure in deformed state.

The kinematic chain consists of a main lever which is driven by a rotary servo actuator and connecting struts which are attached to brackets. The displacement of the main lever is then transferred via kinematical struts which are connected to brackets on the omega shaped stringers (Fig. 6).

3.2. Measurement Equipment

For the measurement of the overall deformation of the flexible leading edge the 3D optical digitizer system “3D Creator” from SenSound is used. For the deformation measurements 18 markers in three different span wise sections are applied to the outside of the skin of the flexible leading edge (Fig. 7).

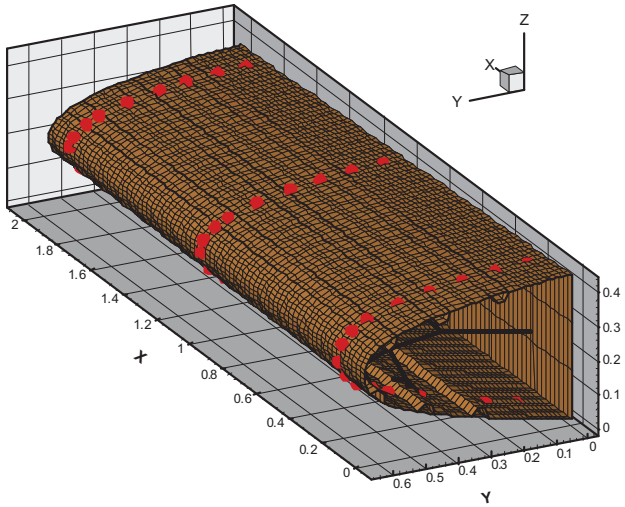

Fig. 7: Position of displacement measurement markers on the outer leading edge skin of the underlying finite element model.

The span wise sections one and three are located at the outer span positions at which kinematic station one and four are mounted. The second section is located between the kinematic stations two and three. Although the "3D Creator" provides a very flexible wireless system for measuring the position of the undeformed and deformed structure, changing of the sensor position is necessary for larger assemblies like the smart droop nose structure. Therefore a reference coordinate system for the measurement of the different sections had to be defined for transformation of the measured data into the global reference coordinate system. The changing of the sensor and transformation in the reference coordinate system had a influence on the measurement accuracy of the system. With the changing of the sensor position the measurement accuracy could be verified to ±2mm.

Besides the position measurements the structural strains are measured at various positions within the skin. Of special interest are the strains at the pre- calculated critical positions. In Fig. 8 a schematic sketch of interesting positions of strain gauges during the tests in chord direction is presented.

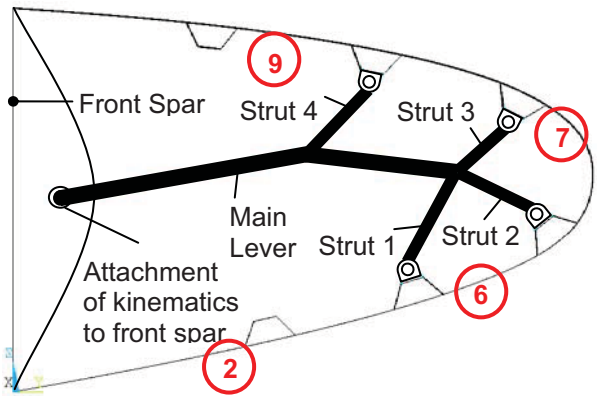

Fig. 8: Schematic sketch of positions of strain gauges at positions of special interest.

In the finite element simulations the position six was identified as most critical location due to the large deformation of the leading edge tip and the change in local bending stiffness which is caused by the step of the thickness from the stringer foot to the thin skin. At this location about 10000 micro strains in circumferential direction of the outer fibers are calculated as maximum strain in deflected position. At the other positions the calculated strains are more moderate with about 3000 to 4000 micro strains.

4. FIRST RESULTS

For a first assessment of the deformed shape of the leading edge, the measured displacements in the ground test are compared to the previously calculated deformation behavior of the smart structure from finite element simulations. The underlying overall finite element model for the comparison of experimental test data is modeled in ANSYS using shell 181 element which are especially suited for the modeling of layered applications. For an accurate assessment of the structural strength all layers of the structure are modeled explicitly. For detection of critical locations and failure of the structure the 2D failure criterion according to Puck was applied for each layer.

The overall model in Fig. 9 consists of the flexible leading edge, the front spar which was developed by CASSIDIAN for attachment of the structure and the four kinematic stations from EADS-IW. The latter are modeled with beam and link elements.

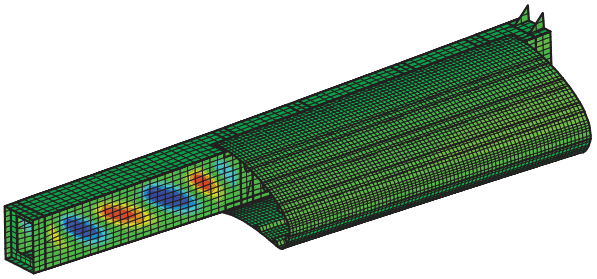

Fig. 9: Combined finite element model of the smart leading edge structure, the test spar and the kinematics, buckling of side walls under 2g wing bending with deflected leading edge.

In order to calculate the deviation of the undeformed structure from the ideal finite element model for reference and to assess the deviations of finite element model and measured coordinates in the ground test, a best-fit approach is used: Because there is no well defined reference edge for the measurements in the ground test setup the measured coordinates from the ground test measurements are transformed by rotational and translational transformation rules into the coordinate system of the finite element model for comparison. Through an optimization of the rotational and translational parameters for the transformation of the measured marker coordinates, the deviation of all three measurement sections from the ideal finite element surface is minimized. The approach is used for the assessment of the deviation of the undeformed structure as well as for the deformation of the structure in deflected state.

4.1. Undeformed Leading Edge Structure

In Fig. 10 and Fig. 11 a comparison of the measured marker positions in undeformed state in the ground test and the position of nodes in the finite element model for section three is presented. In this section the maximum deviation from the ideal state of installation after the optimization is identified. The deviation has its maximum of about -4.6mm at marker 17 which is placed on the lower surface of the leading edge.

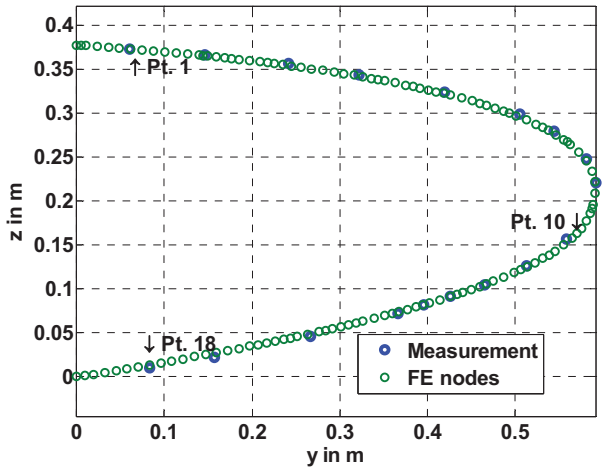

Fig. 10: Comparison of measured coordinates and position of nodes in the finite element model in section three.

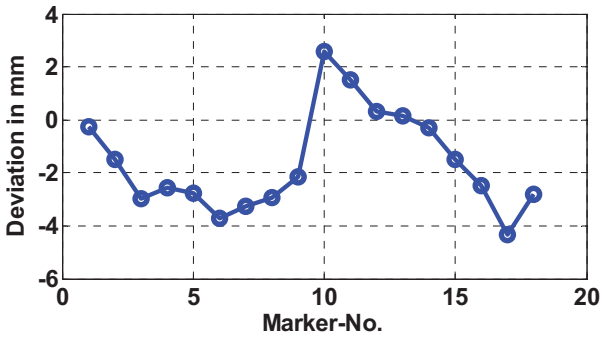

Fig. 11: Distribution of the deviation of the measured coordinates from the finite element node position

The deviations in section three are larger than those in the sections one and two, which are in the order of the measuring accuracy of the optical 3D positioning system. There is still a deviation of more than 4mm between the measured contour of the un-deflected nose and the design shape. The main sources for these discrepancies are manufacturing tolerances of the large hand made composite skin – especially the position of the stringers. It can be concluded that with respect to the measurement accuracy and manufacturing tolerances as well as tolerance problems during assembly the deviations can be classified as minor deviations from the design shape regarding the complexity of the test setup.

4.2. Deformed Leading Edge Structure

In the test program various combinations of leading edge deflection angles and wing bending deformations were tested. In the finite element simulations it was found, that the additional loading from wing bending has only a minor effect on the structural strength. Therefore the most critical load case in terms of structural strength is the deflection of the leading edge to its maximum deflection angle.

4.2.1. Deformations

The maximum deflection angle of the leading edge structure is reached at about 18° deflection of the main lever in Fig. 8. A comparison of the calculated deformation of the smart leading edge structure in fully deflected position and the measured coordinates in the ground test is presented in Fig. 12 and Fig. 13.

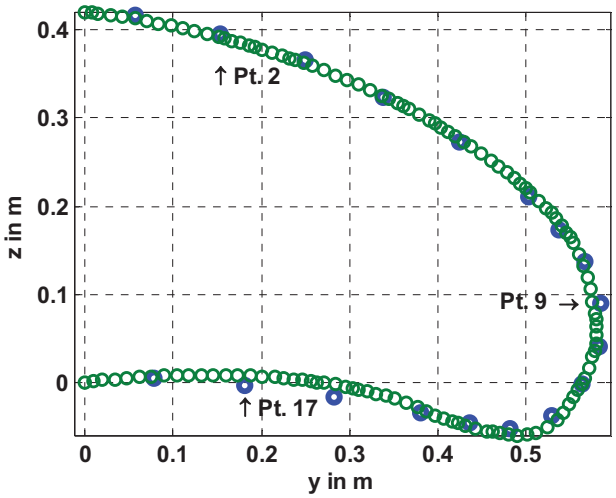

Fig. 12: Deformed section one at x = 161mm (blue) and position of finite element nodes (green) in fully deflected position.

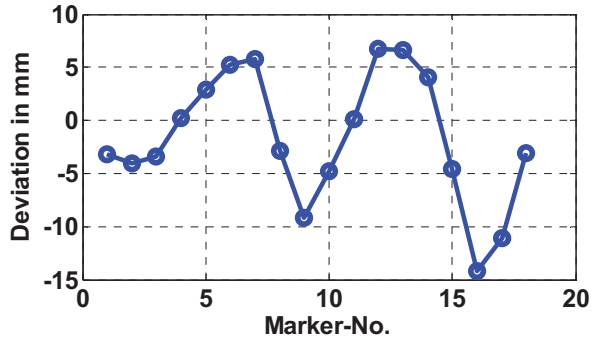

Fig. 13: Distribution of the deviation of the measured coordinates in deformed state from the finite element deformations.

In the fully deflected position the maximum deviation of the calculated shape from finite element analysis can be found in section one with -14.2mm at marker no. 16. A second major deviation occurs at marker no. 9. In the sections two and three the comparison shows good agreement of the calculated finite element shape and the measured data.

The deviations of the measured data from the finite element calculated shape mainly refers to the discrete character of the finite element simulation. While the stiffness distribution in the real leading edge test structure varies continuously, the stiffness distribution in the finite element model is characterized by sudden steps in the

bending stiffness. This is due to the discrete change from (thick) regions of the stringer foot in which the skin thickness plus the thickness of the stringer foot suddenly drops to the minimum thickness of the skin. The effect can clearly be seen in Fig. 12 around marker no. 9. Here the finite element shape (green) in contrast to the measured contour (blue) predicts a local change of curvature at the leading edge tip which forms a region of nearly zero curvature due to the membrane stress during deformation. In the ground test this deformation behavior could not be observed. Due to the continuous stiffness distribution in the real structure the curvature distribution in this region is continuous without any negative local effects. The same is true for the deviation on the lower side of the leading edge around marker 16 and 17. Due to the more continuously deformation behavior of the structure the whole contour of the structure therefore deviates slightly in regions of significant changes in curvature. As mentioned above the additionally applied wing bending had only a minor effect on the deformation behavior of the structure. However, no stability problems of the leading edge structure during the tests were observed.

4.2.2. Strain Measurements without bending

For strain measurements strain gauges were applied at various positions on the outer and inner side of the skin as well as on the struts and the main lever of the kinematics. The main objective of the strain measurements was the measurement of the strains of the outer fibers of the laminate at the pre- calculated critical positions. In the precalculated strain distribution in maximum deflected position, the positions six and seven in Fig. 8 were identified as the most critical locations. For comparison of calculated and measured strains a section between sections two and three at x ≈ 1500mm was chosen. In this section four strain gauges are applied in circumferential direction of the smart leading edge structure. To estimate the strain distribution within the outer fibers of that section the deformation data described in section 4.2.1 was used. The curvature of the deformed structure is calculated from the measurements (see Fig. 14). Using these curvatures the strains are calculated using the following correlation:

$$(1) \quad \varepsilon(\kappa, t) = \frac{1}{2} \cdot t \cdot \kappa .$$

Fig. 15 shows a comparison of measured strains from the strain gauges (black markers), the precalculated strains from FE analysis (red) and the strain calculated from the curvature (blue).

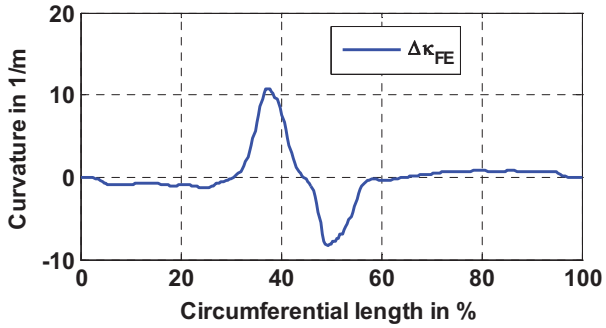

Fig. 14: Curvature of the measured contour of the corresponding section (Q3.5) in the ground test.

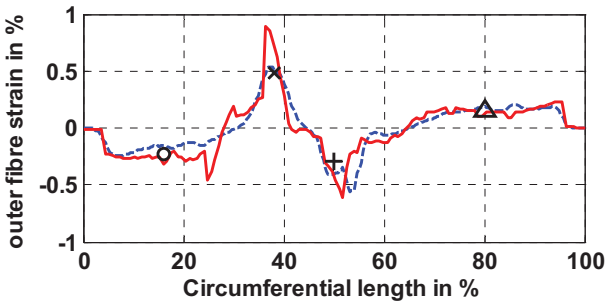

Fig. 15: Comparison of measured and calculated strain in circumferential direction, strains calculated analytically from measured curvature (blue) and from FE analysis (red) with measured strains (black markers) of section Q3.5.

The comparison of the strains at this position shows clearly an over estimation of structural strains in the finite element simulations. While the maximum measured strains at position six (ca. 38% circumferential length) are about 0.5% the finite element analysis predicts maximum strains of 0.8%. The reason for this over estimation of the outer fiber strains is the already mentioned change of stiffness from the stringer flange to the thin skin. Due to the discretization, the skins thickness drops at the position of stringer flanges abruptly to the thickness of the skin which is about 1mm at the leading edges tip. This leads to a large gradient in local bending stiffness and therefore to a concentration of local strains in the finite element analysis. For the comparison of strains in section one, two strain gauges are applied at 38% and 50% of the circumferential length (Fig. 16).

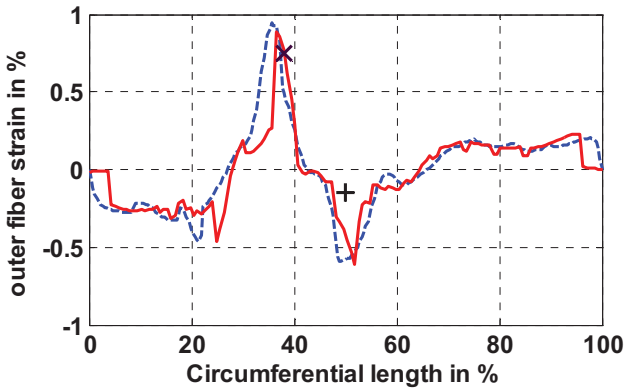

Fig. 16: Comparison of measured and calculated strain in circumferential direction, strains calculated analytically from measured curvature (blue) and from FE analysis (red) with measured strains (black markers) of section Q1.

In both sections the circumferential strain distribution which was calculated from the measured curvature (blue) shows the best agreement with the measured strains. This indicates a successful realization of the concepts idea of the loading of the skin structure with pure bending loads. However, the strain measurements in span wise direction of the strain in circumferential of the outer fibers for the critical position six are summarized in Fig. 17. The presented evolution of strains in different sections of the leading edge shows the strains for a successive increasing

deflection angle of the droop nose device up to the maximum deflection.

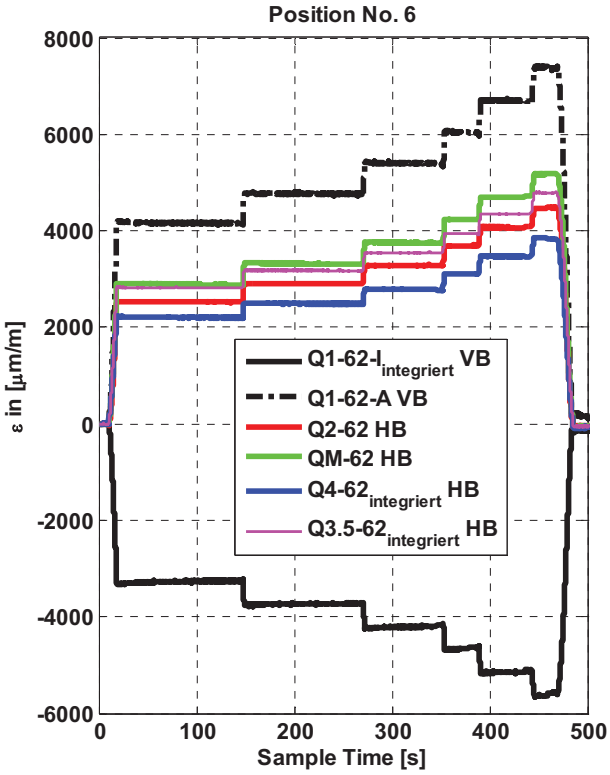

Fig. 17: Overview of strain measurements at various positions in span wise direction of the circumferential strain at position no. 6.

The span wise distribution of the measured strain at the critical position six in Fig. 17 shows the overall maximum strain of the outer fibers of about 7500 micro strains near section one. In comparison with the strain data from the finite element analysis (Fig. 18) the overall trend of decreasing strain at the critical position in span wise direction can be verified.

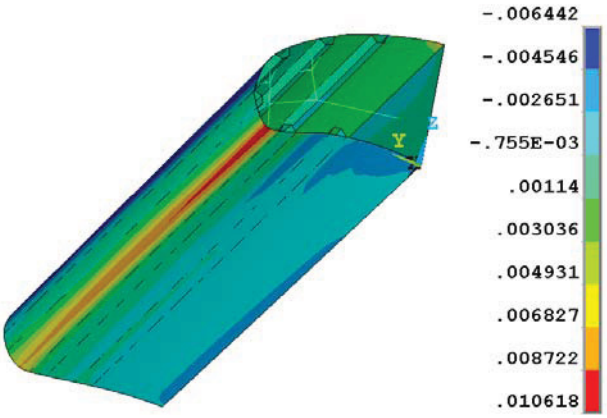

Fig. 18: Circumferential strain in layer one of the 3D test section from finite element analysis, critical strains at position no. 6, strain in Δm/m.

The nomenclature includes the position of the strain gauges in span wise direction with respect to the position of the kinematic stations. For example the maximum strain in circumferential direction can be identified to be in the section at position of the first kinematic station (Q1) at a circumferential length of 62% from the upper front spar position. The measured strain between stations three and four is named section Q3.5. Strain gauge Q1-62-I VB is the only one integrated on the *inner* side of the skin. This explains the negative sign of the values. However the maximum values of the measurements and simulation results show the influence of the discretization in the simulations, again.

Finally the comparison of predicted and measured strains in circumferential direction shows a good agreement of results in large areas of the structure. Even if the absolute maximum values of the finite element simulations are not reached in the experimental tests, there are various reasons for the identified small disagreements in the results. Especially the influence of the characteristic discretization of finite element analysis of fiber reinforced structures and the uncertainty of the position of applied strain gauges play a major role.

4.2.3. Strains under wing bending

Besides the strains under pure deflection of the device without any simulation of wing bending especially the strains with superposed wing bending are of interest. At the test rig the wing bending can be adjusted at three locations in x- direction of the test spar (see Fig. 5): At the end of the spar, at the end of the attached skin and at the position of the third kinematic station. For the adjustment of the predefined and corresponding wing bending lines only small displacements compared to the deflection of the device were necessary. Due to the low measuring accuracy of the 3D Creator system the measured data concerning the bending line of the spar the scattering data had to be smoothed. For the assessment of the large-scale strain distribution in the skin due to the wing bending, the overall finite element model was used to calculate the wing bending deformation using the measured displacements of the test spar.

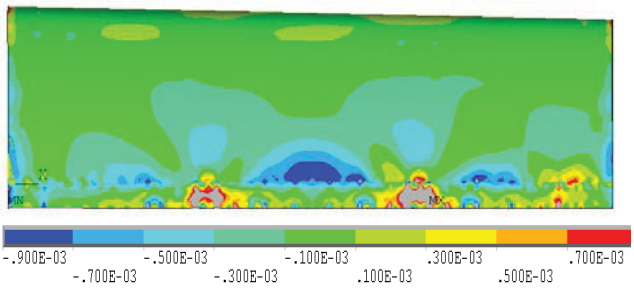

Fig. 19: Strain distribution of the strain in direction of the test spar in the outer fiber layers of the upper skin of the leading edge under simulation of 2.0g wing bending, strain in Δm/m.

The strain distribution in Fig. 19 shows the strain in direction of the test spar in the outer fiber layers of the upper skin of the leading edge. One can see the compression of the upper skin due to the wing bending load. Especially the part of the skin between the middle to kinematic stations is compressed. In span wise direction of the skin endings the value of compression decreases due to the unconstraint edges. Although the test spar showed beginning shear buckling of the sidewalls in the experimental testing under the 2.0g loading and clearly

formation shear buckling in 2.5g loading of the structure, no stability problems of the smart leading edge structure were observed. However, in the experimental tests only a moderate transfer of the spar bending line to the skin could be observed. In the strain distribution of the recalculated overall finite element simulation one can see, that the bending of the spar likewise leads only to very small corresponding strains in the skin. Reason for this can be the way of the attachment of the skin to the spar: As skin-spar interface, solid assembly battens (see Fig. 6) are used for the connection of the skin to the test spar. These battens are riveted in two rows to the skin and to the spar. Certainly the assembly battens provide additional stiffness to the assembled skin in the attachment region. Presumably the large number of joints in combination with the high stiffness of the assembly battens leads to a reduced transfer of the wing bending line to the skin.

In Fig. 20 a detailed view of the evolution of circumferential strain under wing bending in section one (Q1) at position of the kinematic station one at the critical location no. 6 is presented. Due to the fact that the smart leading edge structure has the largest cross-section at the position of kinematic station one, the effect of wing bending on the circumferential strain is here the most obvious one. The presented evolution of the strain shows at the beginning of the measurement a value of about 8600 micro strains in full deflected position under 1.15g wing bending. Then the wing bending is increased until the predefined bending line for 2.0g is reached. With the increasing of the wing bending the strain increases up to nearly 9000 micro strains. After this, the wing bending is reduced to 1.0g bending line and the device is retracted. When compared to other span wise measurements of the strain at the critical position of this load case it can be found that the influence of the wing bending on the circumferential strain decreases with decreasing maximum strain at the critical position which is the case in direction of the smaller cross-sectional area in span direction. The reason for this is the lower stiffness of the large cross-sectional area of the profile at position of the kinematic station one which leads to larger deformations of the profile due to wing bending loads.

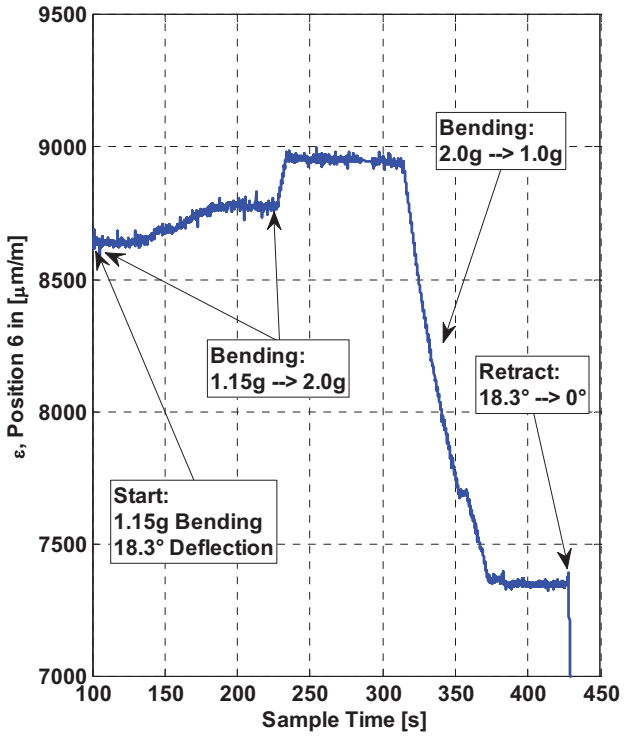

Fig. 20: Detailed view of evolution of circumferential strain under wing bending in section one (Q1) at position of the kinematic station one at the critical location no. 6.

5. DISCUSSION

With respect to the main objective of the ground test, the discussion will focus on the deformation measurements and strain measurements concerning the smart leading edge skin. Besides the test data concerning the skin a detailed analysis of the test data concerning the kinematics is in progress and will be presented in upcoming papers.

5.1. Deformation Measurements

On the basis of the deformation measurements of the smart leading edge structure the desired shape change was verified for three sections along the span of the ground test demonstrator. In the state of installation a maximum deviation of -4.6mm from the underlying finite element model was found. Besides the already mentioned manufacturing tolerances and tolerances from installation effects, the low measurement accuracy of the 3D Creator measurement system (±2mm) and the unconsidered skin thickness (up to ±2.5mm) in the optimization of the transformation parameters play a major role in assessment of the deviations. Therefore the overall calculated deviation in the state of installation can be regarded as a summation of several minor tolerances from the skin, the kinematics, the test spar and the measurement system in which the share can not be clarified definitely due to the low measurement accuracy. The same is true for the measurements of the deformed structure. Even if the local maximum deviation in the deformed position is about -14.2mm, the overall agreement of the shapes is rather good. The deviations in

the deflected position are especially influenced by tolerances of the kinematics which amplify the deviations because of the nonlinear character of the deformation. A drawback besides the low measurement accuracy of the 3D digitizer is the low number of only three slices or section which was measured during the ground tests. Unfortunately the measuring of more slices in span direction within the tight planned test procedure was not possible. A detailed assessment of the surface quality and contour accuracy in span direction was therefore not possible.

5.2. Strain Measurements

Mostly the strain measurements are in good agreement with the precalculated strains from finite element analysis. An exception are the local stress peaks which were identified in the FE analysis at the positions were the omega stringers interfacing with strut one of the kinematics is attached to the skin. In reality and in the FE modeling of the structure the step from the stiffener foot to the skin will certainly lead to a peak in stress and strain. However the step will be more pronounced in the FE analysis due to the discretization. Therefore it was assumed that the strains will be overestimated by the analysis. Furthermore the strain gauges measure only a strain value in a very limited surface area of the structure. Therefore it is unclear if the local strain peaks were successfully covered by strain gauges which were applied in the critical locations.

The very good agreement of the measured strains and the values calculated from the curvature of the profile indicates that the concept idea of the smart leading edge shell structure which is loaded mainly by out of plane bending loads was successfully realized. Otherwise the measured strains would have been beyond the curvature-calculated strain.

The strain measurements under wing bending showed a correlation of the wing bending and the strain in circumferential direction of the structure. It was found that the circumferential strain increases under wing bending. The increase depends on the position in span direction or rather the cross-sectional area of the profile and of course the stiffness distribution along the profile.

6. SUMMARY AND OUTLOOK

First results of a 1:1 ground test of a gap and step less smart leading edge device are presented. The tested leading edge structure is a 2m realistic 3D cutout of an inboard section of the outboard wing of a medium range single-aisle aircraft similar to the A320. In the test program various combinations of leading edge deflection angles and wing bending deformations were tested. In the paper the experimental test data is compared to precalculated finite element analysis.

As the major result of the national project SmartLED the feasibility of a 3D and full scale smart gap and step less high lift device for the leading edge of a transportation aircraft with conventional flight certified materials and a conventional actuation concept was demonstrated. Over the complete test procedure neither structural strength problems nor stability problems were observed. The measurement results of the deformation behavior of the smart structure generally speaking indicate a good agreement with precalculated results of finite element analysis. Local deviations from precalculated results can be assigned to insufficient measurement accuracy during the tests, manufacturing tolerances and tolerance problems during assembly. The measurement results of the strain measurements are also in good agreement with calculated finite element results. Due to the discrete character of the FE simulations in contrast to the continuous stiffness distribution of the realized structure the strains at the critical locations are as expected slightly overestimated. Concerning the measurement accuracy in further tests a 3D digitizer with a measurement accuracy of about the quarter of the minimum skin thickness should be used.

The demonstration of the feasibility of a large scale 1:1 morphing structure with conventional materials in the project SmartLED indicates a starting point for further work in the field of morphing high lift devices at the leading edge as enabler for natural laminar flow wings. In ongoing and upcoming projects like in the European project SADE and Clean- Sky JTI-SFWA subsequently the further development and enhancement of the smart droop nose takes place. While in the project SADE the developed concept of a smart leading edge droop nose will be tested in a full-scale wind tunnel test, the main objective in the JTI-SFWA is to raise the technology readiness level concerning industrialization aspects.

[1] ACARE, “2008 Addendum to the Strategic Research Agenda”, Advisory Council for Aeronautics Research in Europe, 2008.

[2] Kreth, Stefan; König, Reinhard; Wild, Jochen: „Aircraft noise determination of novel wing configurations”, INTER-NOISE 2007, Istanbul, Türkei, 2007.

[3] Pott-Pollenske, Michael; Wild, Jochen: “Entwicklung und Validierung eines Verfahrens zur Beurteilung der Schallabstrahlung von Hochauftriebssystemen“, DAGA 2007, Stuttgart, 2007.

[4] Horstmann, K. H.: “TELFONA, Contribution to Laminar Wing Development for Future Transport Aircraft”, Aeronautical Days, Vienna, 19th-21st June 2006.

[5] Frota, João: “NACRE- An Overview: Towards a Silent-by-Design Aircraft?”, 15th AIAA/CEAS Aeroacoutics Conference, Miami, Florida, 2009.

[6] Zimmer, H.; 1980, Quertriebskörper mit veränderbarer Profilierung, insbesondere Flugzeugtragflügel, Deutsche Patentschrift, DE 29 07 912.

[7] Thill C, Etches J, Bond I. P., Weaver P. M., Potter K. D.: “Morphing Skins – A Review”. The Aeronautical Journal. Vol. 112, No. 1129, pp.117-138.

[8] Campanile, L. F.: “Synthesis of flexible mechanisms for airfoil shape control: a modal procedure”, Proceedings of the 15th International Conference on

Adaptive Structures and Technologies, Bar Harbour, ME, USA, October 24th-27th , 2004.

[9] Kintscher, Markus. “Method for the Pre-Design of a Smart Droop Nose using a Simplex Optimization Scheme”. SAE Aerotech Congress and Exhibition, 10.-12. November 2009, Seattle, Washington, USA.

[10] Monner, Hans Peter und Kintscher, Markus und Lorkowski, Thomas und Storm, Stefan, (2009), Design of a Smart Droop Nose as Leading Edge High Lift System for Transportation Aircraft. AIAA, 5.5. - 7.5. 2009, Palm Spring, USA.